Astron. Astrophys. 146, 95–112 (1985)

ASTRONOMY
AND
ASTROPHYSICS

Spectroscopic analysis of extreme metal-poor "dwarfs"

II. Improved model atmospheres and detailed abundances*

P. Magain**

Institut d'Astrophysique, Université de Liège, 5, avenue de Cointe, B-4200 Cointe-Ougrée, Belgium

Received October 26, accepted December 3, 1984

Summary. We present the results of a spectroscopic analysis of the classical "subdwarfs" HD 19445 and HD 140283 on the basis of new observational material. This analysis makes use of empirical model atmospheres designed to reproduce the observed continuous flux and the Fe I excitation equilibrium. It is shown that these models are also able to reproduce the strong line profiles. The difference between the empirical and theoretical models for these extreme metal-poor dwarfs is tentatively attributed to non-local convection.

We compare the two classical methods of analysis: absolute and differential. We show that the differential analyses of these very weak-lined stars relative to the sun are affected by systematic errors due to the poor knowledge of the damping constants and to the difficulty of locating the continuum in the blue region of the solar spectrum.

The effective temperature and surface gravity are determined by spectroscopic and photometric methods. It turns out that, while HD 19445 is a dwarf star ($\log g = 4.0$), HD 140283 may be classified as a subgiant ($\log g = 3.2$). The trigonometric parallax of HD 140283 is incompatible with its spectroscopic surface gravity. The comparison of the position of these stars in the ($T_{\rm eff}$, $\log g$) diagram with recent isochrones shows that it is nearly impossible to obtain a reasonable age for both stars by using the same value of the mixing length parameter for both.

We have determined the abundances of a number of elements. The main results are the following:

– the iron abundance is lower than indicated by past analyses;

– oxygen is strongly overabundant relative to carbon and iron;

– the "α-elements" magnesium, silicon and calcium are significantly overabundant relative to iron;

– aluminium is overdeficient with respect to magnesium;

– manganese is overdeficient relative to the other iron group elements;

– the behaviour of the *s* elements is in agreement with the conclusions of Spite and Spite (1978);

– strontium is overabundant relative to barium;

– the abundances of sodium and cobalt seem in contradiction with the results for aluminium and manganese.

The implications of these results for the nucleosynthesis and galactic evolution theories are briefly discussed.

Key words: stars: abundances – stars: atmospheres – stars: Population II

Send offprint requests to: P. Magain

* Based on observations carried out at the Haute Provence Observatory, France, and at ESO, La Silla, Chile

** Aspirant du Fonds National Belge de la Recherche Scientifique

1. Introduction

A preliminary analysis of the two well-known metal-poor stars HD 19445 and HD 140283 was reported in an earlier paper (Magain, 1984b = Paper I). This study was based mainly on an analysis of Fe I lines, using the very accurate oscillator strengths of the Oxford group (Blackwell et al., 1982a, and references therein). It was shown that:

(1) the differential analyses of these very weak-lined stars relative to the sun are affected by systematic errors due to the large difference between the solar and stellar equivalent widths;

(2) the continuous fluxes computed from the theoretical model atmospheres do not fit satisfactorily the observed ones. This discrepancy was tentatively attributed to convection which, in the theoretical models, is taken into account through the (rather poor) mixing-length approximation.

One of the aims of the present paper is to re-examine the conclusions of Paper I on the basis of new high quality spectrophotometric observations (Oke and Gunn, 1983) and of an extension of the spectral range towards the ultraviolet, where many interesting lines are present. As will be shown in Sects. 3 and 4, these conclusions are not only confirmed, but also strengthened. The other important goals of this paper are (1) to examine the position of these stars in the HR diagram, in the hope of estimating their mass and age (Sect. 6) and (2) to determine the abundances of a number of elements in their atmospheres in order to test the nucleosynthesis and galactic evolution theories (Sects. 7 and 8).

Before going into the details of the analysis, it may be useful to make our position on the question of spectroscopic analysis of halo stars as clear as possible. Our analysis is in some ways extremely classical: we use photographic spectra, plane parallel model atmospheres and the assumption of local thermodynamic equilibrium (LTE). The choice of the stars is itself classical: these are the well-known "subdwarfs" analysed by Aller and Greenstein (1960) and a number of other authors (see Table 1 of Paper I). Less classical for papers dealing with metal-poor stars are the number of stars considered (two) and the quality of the spectral material used. The higher quality of our data is demonstrated in Paper I and in the next section (see also Magain, 1984a, for a more complete discussion). This higher quality of our spectra naturally called for a more ambitious analysis: some assumptions of past analyses may be tested, finer effects may be discovered. So, the

main aim of this paper is to realise a detailed and accurate analysis of a very limited number of representative halo dwarfs. It is clear that the loss of a statistically significant sample is a handicap when comparing the results with the predictions of galactic evolution theories. But we believe that the careful analysis of a small number of representative stars is absolutely essential for several reasons. First, rough analyses of a large number of stars (e.g. by photometry or low dispersion spectroscopy) must be calibrated on a certain number of carefully analysed standard stars covering the range (of effective temperature, surface gravity, chemical composition, ...) considered. Moreover, these rough analyses are generally based on a certain number of assumptions (such as a common deficiency of all heavy elements, or a constant microturbulent velocity) which must be confirmed, or invalidated, by detailed analyses. And last, but not least, careful detailed analyses with high quality data may (and do) reveal effects which are overlooked by rougher studies – in which we include many high dispersion analyses, in particular those based on a single noisy spectrum. Among these effects, we may mention the systematic errors in differential analyses, the discrepancy between the observed continuous fluxes and the predictions of theoretical model atmospheres or the (probably related) discrepancy between the Fe I excitation equilibrium and the photometry [similar effects reported earlier in the literature were due to errors in the laboratory oscillator strengths (Peterson and Carney, 1979) or in the methods of analysis]. Finally, as long as the relative abundances are concerned, many interesting variations are within a factor two and need a high quality analysis to be unambiguously demonstrated. It will be shown, in the last sections, that an accuracy much better than a factor two is within the reach of a careful analysis, even for these rather faint stars. In the classification introduced by Pagel (see Gustafsson, 1980) between "ultimate refiners" and "broad sweepers", we certainly fall in the first category.

2. Spectral data

The observational material and reduction procedure were briefly described in Paper I. For the present analysis, the Haute Provence Observatory (OHP) plates were recorded in the near ultraviolet in order to extend the spectral range and to include lines of elements poorly represented in the blue. So, the OHP data consist in 19 baked IIa-O plates with a reciprocal dispersion of 12.4 Å mm^{-1}, corresponding to a resolution of about 0.25 Å. The 9 plates of HD 19445 were recorded from 3500 to 4900 Å, while the 10 plates of HD 140283 were usable from 3700 to 4900 Å. The data for HD 140283 are supplemented by 6 baked IIa-O plates from the 1.52 m ESO telescope at La Silla (Chile), with the same reciprocal dispersion. These 6 plates were recorded from 3500 to 4200 Å. The different spectra of the same set were finally co-added in order to increase the signal-to-noise ratio (see Paper I).

A plot of ESO versus OHP equivalent widths for the range in common reveals a systematic difference between these two sets of data, the ESO equivalent widths being some 10% larger than the corresponding OHP data (Fig. 1). Using 25 lines in the range 4000 Å $< \lambda <$ 4200 Å, we find by least squares fitting:

$$W_\lambda(\mathrm{OHP}) \simeq 0.88\, W_\lambda(\mathrm{ESO}) + 1.8\,, \qquad (1)$$

where the equivalent widths are measured in mÅ.

This discrepancy (as similar ones in the comparison of data from different authors, see Magain, 1984a) called for a deeper

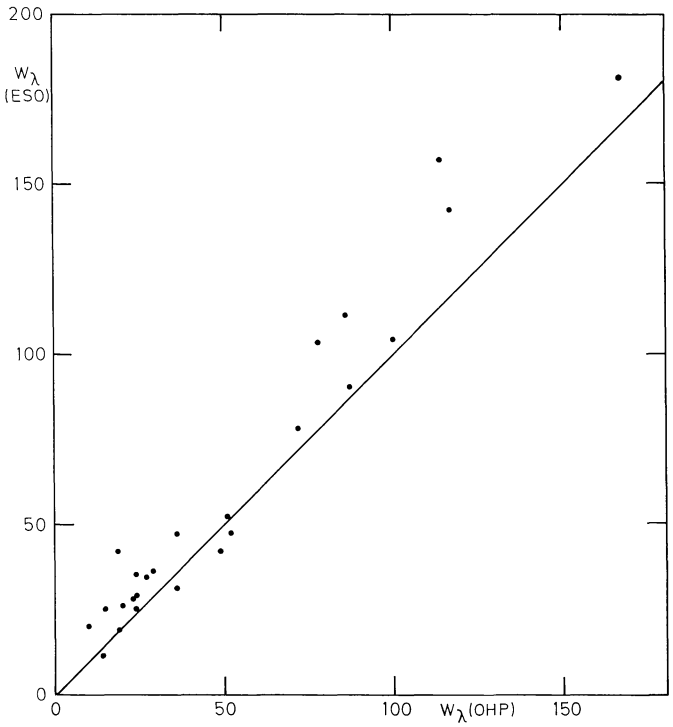

Fig. 1. Comparison of the equivalent widths measured on ESO and OHP spectra for HD 140283. All equivalent widths are in mÅ

investigation of the possible systematic errors in our equivalent widths. To this end, we obtained at OHP nine spectra of the sunlight, reflected by the moon or by Mars, or scattered by the terrestrial atmosphere. These solar spectra were obtained with the same instrument as the stellar spectra, in the same conditions, and reduced in exactly the same way. The use of neutral filters allowed us to obtain an exposure time comparable to the stellar ones. These nine spectra were co-added in the same way as the stellar spectra and compared to the high resolution, low noise spectrum of the solar irradiance obtained at Sacramento Peak Observatory by Beckers et al. (1976). Since at a resolution of 0.25 Å the crowding of the lines in the blue region of the solar spectrum prevents to locate accurately the continuum, it is meaningless to compare "equivalent widths" measured on these two spectra. Moreover, this problem of continuum location being absent from the metal-poor stars spectra, it is desirable to avoid it in the comparison of the solar spectra. So, we convoluted the Sacramento Peak spectrum with the instrumental profile of our spectra (approximated by a Gaussian of empirically determined width) before comparison. This comparison is displayed in Fig. 2 for a typical spectral region. The agreement is very satisfactory, indicating that the OHP data are probably free of any significant systematic error. So, we must conclude that the ESO equivalent widths are overestimated by some 10%. The source of this error is unknown to us, but we might suspect the calibration plates which are not of the highest quality in this particular case.

The internal accuracies of the different sets of equivalent widths for the two stars in question were compared in Paper I where it was shown that our data are superior to previously published ones. A more detailed discussion may be found in Magain (1984a). The equivalent widths measured on our spectra are listed in the Appendix.

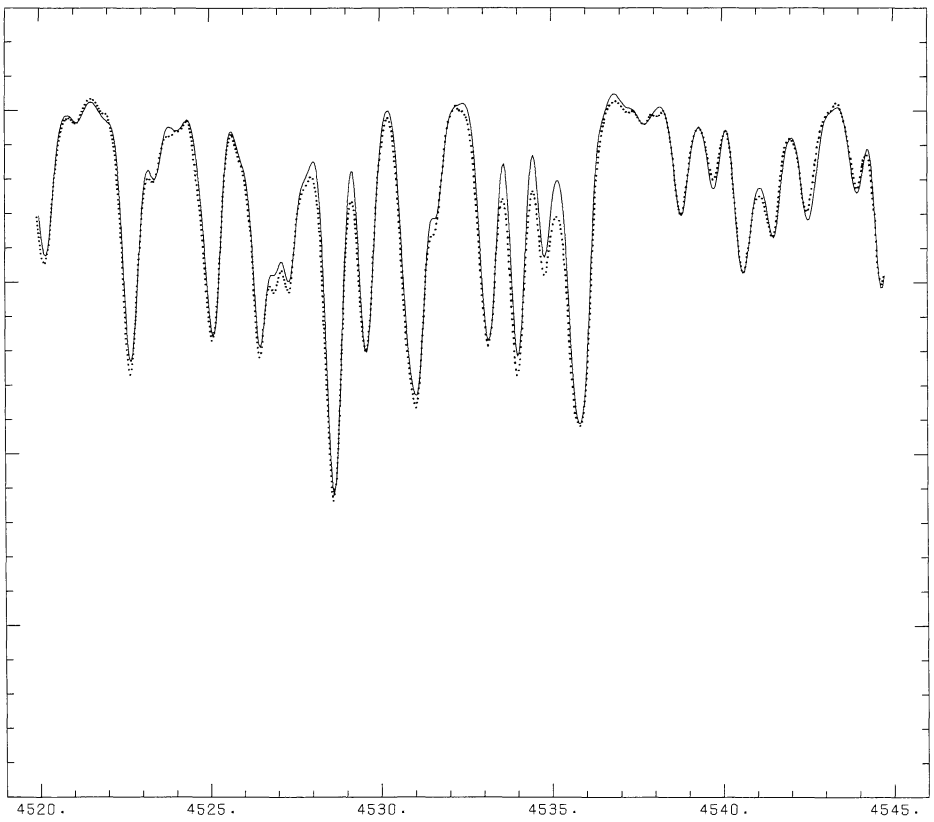

Fig. 2. Comparison of a typical region of the solar spectrum obtained at OHP (dotted line) with the convolved Sacramento Peak spectrum (full line)

3. Construction of empirical model atmospheres

As was shown in Paper I, the theoretical (flux constant) model atmospheres fail to reproduce the observed continuous flux of these stars. This conclusion is based on two independent observations:

(1) the effective temperature obtained from blue-visual colour indices is some 200 K higher than the temperature deduced from the red-infrared indices;

(2) when a model is selected so as to reproduce the spectrophotometric observations in the red-infrared, the model continuous flux is lower than the observations in the blue-violet.

These two observations may be considered as independent since the calibration of the colour indices (see, e.g., Magain, 1983) is completely independent from the calibration of the spectrophotometry. However, the conclusions of Paper I were based mainly on spectrophotometric data published before 1983. Since then, very high quality observations have been reported by Oke and Gunn (1983), so we are now able to carry out a more detailed analysis of the discrepancy. In order to avoid any additional uncertainty coming from the absorption lines, we have corrected the Oke and Gunn observations for the line blanketing by measuring on our spectra the fraction of the flux blocked by the lines in the scanner bands shortwards of 4900 Å. At longer wavelengths, we selected the scanner bands in which the line absorption was found to be negligible by comparison with the solar spectrum. Note that in the whole spectral range, the bands containing strong lines were rejected, so that the correction for line absorption never exceeds 0.05 mag.

When the data are compared to the continuous fluxes predicted by the most sophisticated model atmospheres available

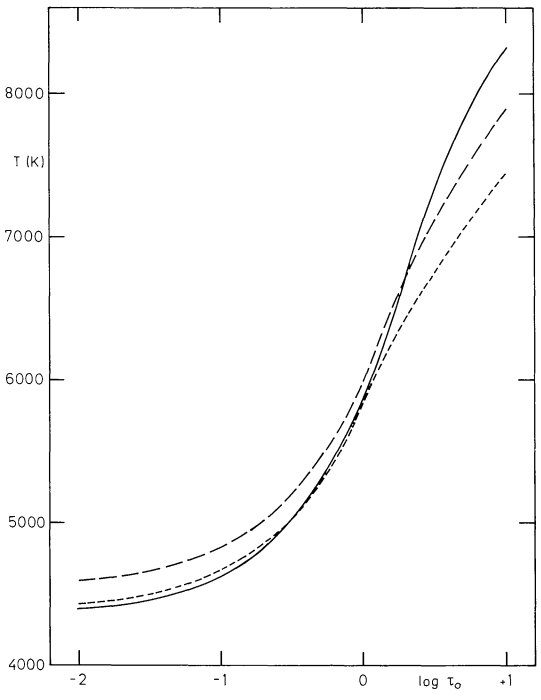

Fig. 3. Comparison of the temperature distributions of the different models of HD 19445. Full line: empirical model. Long dashes: theoretical model selected to match the spectrophotometric observations. Short dashes: theoretical model reproducing the Fe I excitation equilibrium

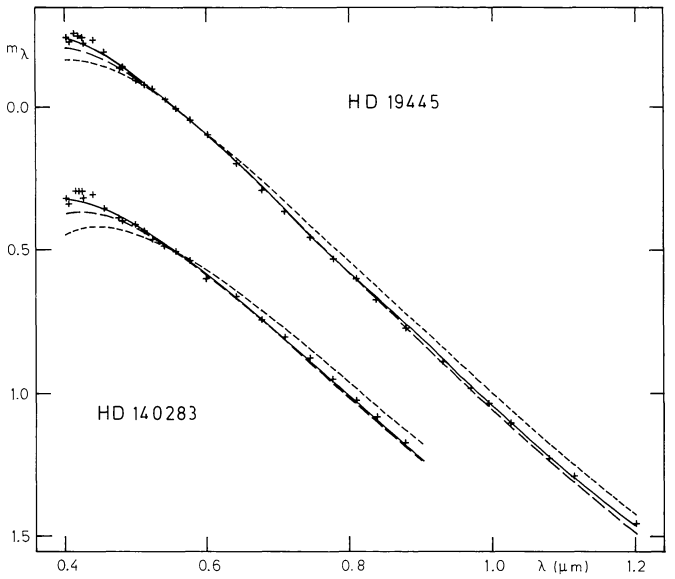

Fig. 4. The corrected Oke and Gunn observations (crosses) are compared with the continuous fluxes predicted by the different models, normalised at 5560 Å. See Fig. 3 for the meaning of the different curves

(Gustafsson et al., 1975; Kurucz, 1979), the discrepancy mentioned in Paper I clearly appears (Fig. 4). It may be described in the following way. If a model is selected in order to match the observed continuous flux in a limited spectral range (say, a 2000 Å interval), the effective temperature obtained increases as the selected spectral range is shifted towards the blue. Since, in this spectral region, the flux at shorter wavelengths originates from deeper layers in the atmosphere (due to a decrease of the continuous opacity towards the blue), this observation seems to indicate that the theoretical model atmospheres underestimate the temperature gradient in the layers contributing to the bulk of the continuous flux. But, in the stars considered here, these layers correspond to the top of the convection zone, which is just the region where the mixing-length "theory" of convection is most inaccurate. So, we may conclude that the discrepancy between theory and observation is probably due to non-local effects at the top of the convection zone. Before a satisfactory theory of convection is available, the best we can do is to replace the theoretical models by empirical ones designed to match as many observations as possible.

We have devised a method to determine the temperature distribution in the layers contributing to the bulk of the continuous flux. The continuous flux at wavelength λ may be computed from:

$$F_\lambda^{\rm calc} = 2\pi \ln 10 \int_{-\infty}^{+\infty} S_\lambda(\tau_0) E_2(\tau_\lambda) \frac{\kappa_\lambda}{\kappa_0} \tau_0 \, d\log\tau_0 , \qquad (2)$$

where τ_λ is the optical depth at wavelength λ and τ_0 the standard optical depth (here, at $\lambda_0 = 5000$ Å) and $\kappa_\lambda(\kappa_0)$ is the continuous opacity at wavelength $\lambda(\lambda_0)$. $E_2(\tau)$ is the exponential integral (see, e.g., Gray, 1976) and $S_\lambda(\tau)$ the source function.

The principle of our method is the following. We start with a trial model, from which we compute the continuous flux $F_\lambda^{\rm calc}$ via Eq. (2). We then compare it to the observations $F_\lambda^{\rm obs}$ and compute the flux errors:

$$\delta f_\lambda = (F_\lambda^{\rm obs} - F_\lambda^{\rm calc})/F_r . \qquad (3)$$

(Since the absolute scale of the observed flux at the stellar surface is not known, it is necessary to work relative to the flux F_r at a certain reference wavelength λ_r.) The corrections of the temperature distribution are then derived from the flux errors by differentiating Eq. (2). We get

$$\delta f_\lambda = \int_{-\infty}^{+\infty} K(\lambda, x) \delta T(x) \, dx , \qquad (4)$$

where $x = \log\tau_0$, $\delta T(x)$ is the temperature correction and

$$K(\lambda, x) = 2\pi \ln 10 \frac{\partial B_\lambda}{\partial T} E_2(\tau_\lambda) \frac{\kappa_\lambda}{\kappa_0} \frac{\tau_0}{F_r} . \qquad (5)$$

In computing $K(\lambda, x)$, we have made several approximations: we have assumed that the source function is equal to the Planck function $B_\lambda(T)$ and that the variations of $E_2(\tau_\lambda)$ and κ_λ/κ_0 with temperature are negligible compared to the variation of the Planck function. We adopt an iterative procedure in which the correction $\delta T(x)$ is used to compute a better model from which new flux errors are obtained, and so on. Thus, the approximations in the computation of $K(\lambda, x)$ (but not in the computation of $F_\lambda^{\rm calc}$) may alter the rate of convergence but not the final solution. Note that the determination of $\delta T(x)$ from Eq. (4) is, as many inverse problems, an "ill-posed problem", i.e. a small error on δf_λ induces an enormous error on $\delta T(x)$. To solve such a problem, we must impose some additional constraint on $\delta T(x)$. A natural constraint in such an iterative procedure is to force $\delta T(x)$ to be sufficiently small. The problem is then solved by least squares after discretization, minimizing the quantity:

$$\mathcal{S} = \sum_i \left[\sum_j K_{ij} \delta T_j - \delta f_i \right]^2 + \eta \sum_j \delta T_j^2 , \qquad (6)$$

where index i refers to the different wavelengths of observation and index j to the different depth points. η is a parameter which determines the relative importance of the two terms in Eq. (6). As η increases, the stability of the solution is improved but the rate of convergence is decreased. By varying the parameter η and the starting temperature distribution, we have checked that this method leads to an unambiguous solution in the region $-0.5 \lesssim \log\tau_0 \lesssim +0.5$, that is in the layers where the bulk of the continuous flux is formed (Magain, 1984a). In the shallower layers, we determine the temperature by requiring the Fe I excitation equilibrium to be satisfied. [The detailed form of the $T(\tau)$ relation in these layers is fixed by comparison with the temperature distribution of the theoretical Gustafsson models, assuming that convection has a negligible effect there.]

In Fig. 3, the empirical temperature distribution for HD 19445 is compared with the $T(\tau)$ relations of two theoretical Gustafsson models: the first reproducing the Fe I excitation equilibrium and the second giving the best match to the continuous flux in the region 5000 Å $< \lambda <$ 12,000 Å. The empirical model for HD 140283 is nearly identical, given the difference in effective temperature between the two stars. The continuous fluxes predicted by the different models discussed above are compared with the Oke and Gunn (1983) observations in Fig. 4, while Fig. 5 shows that the empirical models also reproduce very well the H_β line wings. The situation is the same for other Balmer lines. The hydrogen line wings being primarily sensitive to the temperature structure of the deeper layers, this excellent agreement confirms the validity of the models built from the continuous flux. As Fig. 6 shows, these empirical models also very satisfactorily reproduce the Ca II K line profile, which is sensitive to the form of the $T(\tau)$ relation through the whole atmosphere. The surface gravity used in computing

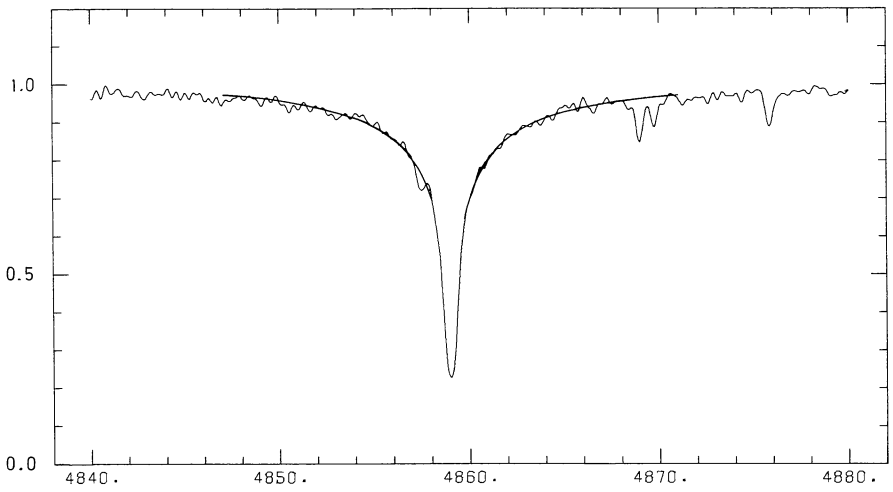

Fig. 5. The H_β profile of HD 19445 is compared with the calculation using the empirical model. Note the wavelength shift due to the large radial velocity of the star

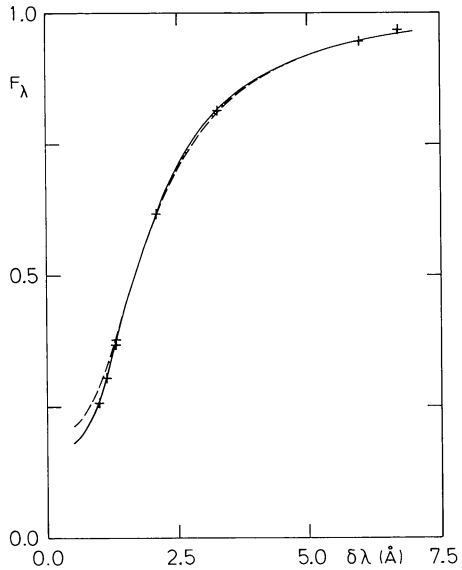

Fig. 6. Comparison of the profile of the Ca II K line of HD 19445 (crosses) with the predictions of the empirical model (full curve) and of the theoretical model selected from the photometry (dashed curve)

these profiles was determined from independent criteria, and the Ca abundance was deduced from weak Ca I lines (see Sect. 5). The discrepancy occurring in the line core may be attributed either to non-LTE effects or to errors in the observed profile (the photographic calibration being most delicate in the very low exposure region). Note that this discrepancy is stronger when the theoretical models are used to compute the line profile. Once more, the empirical models give the best fit to the observations.

In summary, we may conclude that the empirical models designed to reproduce the observed continuous flux and the Fe I excitation equilibrium provide the best fit to the bulk of available observations. Although they were not at all designed to reproduce line profiles, they prove able to fit very well both the Balmer line wings and the K line of Ca II. On the other hand, as most model atmospheres available up to now, they are based on a certain number of strong assumptions, such as plane parallel stratification. If, as we feel, convection plays an important role in these stars, it may not be safe to neglect temperature inhomogeneities or turbulence phenomena. However, the quality of the available data does not warrant to go much further in sophistication. It may be the time to recall that similar plane-parallel empirical models, such as the Holweger-Müller (1974) model, are extremely successful in solar spectroscopic analyses (see, e.g., Sauval et al., 1984; Grevesse, 1984). Finally, we should add (as was already noted in Paper I) that the results of the spectroscopic analysis using the empirical model are not significantly different from the results of the analysis with a theoretical model, as long as the latter is selected in order to satisfy the Fe I excitation equilibrium.

4. Methods of line analysis

As in Paper I, we use a detailed line-by-line analysis, the line abundances being computed in order to reproduce the observed equivalent widths. The computer program is not the same as the Meudon program used in Paper I, but is based on the same assumptions, mainly local thermodynamic equilibrium (LTE). We have checked that the two programs give essentially the same results for the stars considered here.

An important conclusion of Paper I was that the differential analyses of these very weak-lined stars relative to the sun are subject to important systematic errors, due to the large difference between the solar and stellar equivalent widths. The source of these large errors (sometimes more than a factor two) was identified as a wrong choice of the damping constants, affecting the solar line abundances and, thus, the stellar abundance relative to the sun. However, although correct, this explanation is only part of the truth, especially when the analysis is based on the blue spectral range, where the crowding of the lines in the solar spectrum may add significant errors.

To illustrate this, consider the sixteen Fe I lines used in the HD 19445 analysis of Paper I. Since these lines are reasonably weak in the star and since no crowding or continuum location problem is present in the stellar spectrum, the stellar absolute Fe abundance is practically independent of the choice of the damping constants and, of course, completely independent of any problem in the determination of the solar equivalent widths. So, any error in [Fe/H], that is in the stellar Fe abundance relative to the sun, arises essentially from an error in the solar absolute Fe abundance, as deduced from the set of lines considered (i.e. the lines well suited for the *stellar* analysis). Accordingly, the errors in the stellar [Fe/H] due to the use of a differential analysis may be investigated by considering the solar spectrum alone.

To carry out the solar analysis, we use the Holweger-Müller (1974) model with a microturbulent velocity of $0.9\,\mathrm{km\,s^{-1}}$ at the center of the solar disk. We compute the abundances for the 16 lines considered, using the Oxford oscillator strengths. Let us recall that the solar Fe abundance obtained from this set of oscillator strengths and the same model and computer program is $\log A_{\mathrm{Fe}}=7.65$ (in the usual scale $\log A_{\mathrm{H}}=12.00$) when weak Fe I lines are used. We shall adopt this figure as the correct solar Fe abundance.

Let us now compute the solar Fe abundance from the set of 16 (rather strong) lines used in the differential analysis. First, we use the equivalent widths of the MMH catalogue (Moore et al., 1966). If we adopt a damping constant γ_6 increased 2.5 times over the Unsöld formula (Gray, 1976), i.e. $f_6=2.5$, we obtain $\log A=7.17\pm0.17$ (standard deviation), that is a factor 3 below the correct value, for a standard choice of the damping constants. Choosing $f_6=1$ leads to $\log A=7.46\pm0.20$. Thus, an uncertainty of a factor 2.5 in γ_6 produces an uncertainty of a factor 2 on the solar Fe abundance. Adopting the damping constants of Simmons and Blackwell (1982) leads to $\log A=7.41\pm0.20$, which means that a systematic error of -0.24 dex remains when the best damping constants are used.

Since the MMH equivalent widths are affected by non negligible errors, the next step consists in measuring the equivalent widths on a high resolution, low noise solar spectrum. Here we use the Liège atlas (Delbouille et al., 1973). Among the 16 lines considered, we find that 9 are too badly blended to be measurable with acceptable accuracy (which may not be found, of course, by simply consulting the MMH catalogue). Using the 7 remaining lines, we find $\log A=7.51\pm0.08$ with the Simmons and Blackwell damping constants. Note that for the same 7 lines, the MMH equivalent widths lead to $\log A=7.36\pm0.12$, so the use of better data leads to a reduction of both the systematic and random errors.

Even with these improved equivalent widths, a discrepancy of 0.14 dex thus remains, which is unacceptably large for a careful solar analysis. On closer examination, it appears that the continuum is not well defined in the vicinity of 6 of these lines (out of 7!). Only high points are measurable, but no "flat portion" reminiscent of a continuum. Since there is no reason to believe that these high points are located on the continuum, and not below, the local continuum drawn through these points will generally be lower than the true continuum. This will result in a systematic underestimate of the solar equivalent widths. If we use the single line with a relatively well defined local continuum (λ 4489.75), we obtain $\log A=7.64$, in excellent agreement with the adopted value.

It appears therefore that the differential and absolute analyses will give the same result provided that:

(1) good damping constants are used;

(2) the solar equivalent widths are carefully measured on a high resolution, low noise spectrum;

(3) only unblended lines with a well defined local continuum are used (in both the solar and stellar spectra).

This may seem trivial but is practically never realised in spectroscopic analyses of such stars. The example above shows that condition (3) drastically reduces the number of lines which may be used (here, from 16 to 1). In many cases, no line will satisfy entirely this condition. And, if some do, the problem of the damping constants will generally still be there. These drawbacks of the differential analyses prompt us to rely on experimental oscillator strengths and, thus, to realise an absolute analysis. This is easy in the case of Fe I, for which very accurate oscillator strengths are available (Blackwell et al., 1982a, and references therein), but the situation may be much less favourable for other atoms or ions.

5. Determination of the physical parameters

This section is concerned with the determination of the so-called "physical parameters" of the atmospheres of the stars in question, namely effective temperature T_{eff}, surface gravity g and microturbulent velocity v_t.

5.1. *Microturbulent velocity*

The microturbulent velocity is determined by requiring the deduced abundance to be independent of the line equivalent width. We use the Fe I lines listed in Table 2 of Paper I (except the 2.2 eV lines, see Blackwell et al., 1984a). In order to avoid the systematic error discussed in Magain (1984c), the procedure recommended in that paper is adopted, i.e. we plot the line abundances versus theoretical equivalent widths instead of observed ones. We obtain $v_t=1.4\,\mathrm{km\,s^{-1}}$ for HD 19445 and $1.5\,\mathrm{km\,s^{-1}}$ for HD 140283.

5.2. *Effective temperature*

(1) We first determine the effective temperature by computing the integrated flux emitted by the empirical model atmospheres discussed in Sect. 3. The correction for line blanketing is carried out in the same way as in Paper I, i.e. by comparing the integrated continuous flux of the empirical model with the corresponding quantity for the theoretical model and assuming that the fraction of the flux blocked by the lines is the same in both models.

(2) The effective temperature is also determined by the infrared flux method (Blackwell and Shallis, 1977; Magain, 1984a). The integrated flux is computed from the Oke and Gunn (1983) data, supplemented by IUE spectra shortwards of 3080 Å.

(3) Third, the effective temperature is derived from the $V-K$ colours as given by Carney (1983), with the calibration of that author.

The T_{eff} values deduced by these three methods are summarized in Table 1. The adopted uncertainties take into account the uncertainty of each method as well as the very good agreement between the different determinations.

5.3. *Surface gravity*

(1) The surface gravity may be determined from the Fe ionization equilibrium: the same Fe abundance should be deduced from the two stages of ionization. The main uncertainty of this method,

Table 1. Effective temperature

Method	T_{eff} (K)	
	HD 19445	HD 140283
(1) Integrated flux	5890	5515
(2) Infrared flux	5885	5590
(3) $V-K$ colour	5900	5580
Adopted value:	5890 ($\pm$ 60)	5570 ($\pm$ 100)

apart from possible non-LTE effects, comes from the rather poor accuracy of the Fe II oscillator strengths. In order to test the internal accuracy of the different sets of published Fe II oscillator strengths, we have computed the dispersion of the abundances deduced from the different Fe II lines measured on our spectra. It appears that the data of Moity (1983) are best suited for our purpose since this author gives oscillator strengths for all the lines considered and since their internal accuracy is among the best. Since any error on the absolute scale of these oscillator strengths would produce a systematic error on the deduced surface gravities, the accuracy of the absolute scale is even more important that their internal accuracy. We have checked the absolute scale by comparing the lifetimes deduced from Moity's data for six Fe II levels to the values measured by Hannaford and Lowe (1982). This comparison indicates a systematic overestimate of Moity's oscillator strengths: $\delta \log(gf) = 0.07 \pm 0.04$. Accordingly, all Fe II oscillator strengths have been reduced by 0.07 dex. This correction corresponds to a difference of 0.2 dex on the deduced surface gravity.

(2) We have used the Ti ionization equilibrium in a similar way. The oscillator strengths of Ti I lines are taken from Blackwell et al. (1982c). For Ti II, we consider the measures of Danzmann and Kock (1980), Wolnik and Berthel (1973), the computations of Kurucz and Peytremann (1975) and the compilation of Wiese and Fuhr (1975). We adopt the absolute scale of Danzmann and Kock, with a small correction of -0.02 dex, as determined by Blackwell et al. (1982b). The adopted values are listed in the Appendix.

(3) Third, the surface gravity is deduced from strong Fe I lines with Oxford oscillator strengths. The damping constants are taken from Simmons and Blackwell (1982). These values were determined from fits of the solar line profiles. The strong Fe I lines used for the surface gravity determination are listed in Table 2, along with the gravity indicated by each line. These values are obtained by forcing the abundance deduced from the strong line to equal the value indicated by the weak Fe I lines. In the two stars, the 4045.8 Å line indicates a surface gravity significantly higher than the other lines. We were not able to find the source of this discrepancy and attributed half weight to that line.

(4) The same method is applied to the strong resonance line of Ca I at 4226.7 Å. Its oscillator strength is well known from lifetime measurements (Wiese and Martin, 1980). Its damping constant is determined from a fit of the solar line profile, with a solar Ca abundance $\log A_{Ca} = 6.36$ (Smith, 1981). We obtain an enhancement factor $f_6 = 1.6$ over the Unsöld value. The stellar Ca abundance is determined from 4 weak Ca I lines, with the oscillator strengths of Smith and O'Neill (1975).

(5) We have also fitted the profile of the K line of Ca II, using the same Ca abundance as above, an oscillator strength $\log(gf) = 0.135$ (Wiese and Martin, 1980) and a damping enhancement factor $f_6 = 1.5$ determined from a fit of the solar line.

(6) The surface gravity is also determined from a measure of the Balmer discontinuity. From the Oke and Gunn (1983) spectrophotometric observations, we compute the quantity

$$D = m_c(3560) - \tfrac{1}{2}[m_c(4020) + m_c(4060)], \quad (6)$$

where $m_c(\lambda)$ is the magnitude of the continuum in the scanner band centered on wavelength λ. This continuum magnitude is calculated by correcting the Oke and Gunn measurements for the line absorption as measured on our spectra. The surface gravity is then determined by forcing the model to give the right value of D.

The values of the surface gravity deduced from these six methods are listed in Table 3. Considering the typical uncertainty of a single determination ($\delta \log g \simeq 0.3$), the agreement between the six different determinations is excellent. Note that the quoted error bars take into account this excellent agreement as well as the typical uncertainty of each single value. The physical parameters of the two stars are summarized in Table 4.

Table 2. Gravity from strong Fe I lines

λ	f_6	log g	
		HD 19445	HD 140283
3820.4	1.1	3.92	3.22
3825.9	1.1	3.90	3.33
3859.9	1.0	4.03	3.25
4045.8	1.2	4.32	3.68
4071.8	1.2	4.19	
4271.8	1.2	4.07	
4383.6	1.2	4.17	

Table 3. Surface gravity

Method	log g	
	HD 19445	HD 140283
(1) Fe ioniz. equil.	3.9	3.0
(2) Ti ioniz. equil.	3.8	3.2
(3) Strong Fe I lines	4.1	3.3
(4) Strong Ca I line	4.2	3.1
(5) K line profile	3.9	3.3
(6) Balmer discont.	4.2	3.3
Adopted value:	4.0 ($\pm$0.2)	3.2 ($\pm$0.2)

Table 4. Physical parameters

	HD 19445	HD 140283
T_{eff} (K)	5890 ($\pm$60)	5570 ($\pm$100)
log g (cm s^{-2})	4.0 ($\pm$0.2)	3.2 ($\pm$0.2)
v_t (km s^{-1})	1.4 ($\pm$0.2)	1.5 ($\pm$0.2)

6. Mass and age

Once the effective temperature and surface gravity are known, the mass of the star may be determined by two different methods. In the first method ("method of the parallax"), the angular diameter ϕ is determined by the infrared flux method (Blackwell and Shallis, 1977; Magain, 1984a). Combined with the trigonometric parallax π, the angular diameter gives the stellar radius R which, along with the surface gravity (determined by spectroscopic means), allows to compute the stellar mass. The relevant data are summarized in Table 5. The parallax of HD 19445 is taken from Jenkins (1952). For HD 140283, this catalogue lists three determinations, from Yale (0.052 ± 0.011), Cape (0.034 ± 0.012) and McCormick (0.010 ± 0.011) Observatories. However, a more recent determination from the McCormick Observatory has been published since

Table 5. Data for the computation of the stellar masses

	HD 19445	HD 140283
π (arcsec)	0.021 ± 0.006	0.050 ± 0.012
$\phi (10^{-3}$ arcsec)	0.22 ± 0.02	0.36 ± 0.03
$R/R_\odot$	$1.1 \, {}^{+0.6}_{-0.3}$	$0.8 \, {}^{+0.3}_{-0.2}$
$M/M_\odot$	$0.46^{+1.2}_{-0.3}$	$0.03^{+0.07}_{-0.02}$

Table 6. Mass and age deduced from the ($T_{\rm eff}$, log$g$) diagram

	HD 19445	HD 140283
Mass ($M_\odot$)	0.7 ± 0.1	1.1 ± 0.3
Age (10^9 yr)	22 ± 10	$4.5^{+5.0}_{-2.0}$

(Ianna and McAlister, 1974). These authors give $\pi = 0.057 \pm 0.009$, a value which differs considerably from the one previously determined at that Observatory. Since the authors do not comment on the discrepancy, we have adopted their more recent value instead of the older one and computed a mean of that value with the Yale and Cape determinations, following the Jenkins procedure. This mean is the value listed in Table 5. Combined with the spectroscopic gravity, this parallax implies a ridiculous mass for HD 140283. This seems to indicate that either the trigonometric parallax or the spectroscopic gravity is wrong. Let us recall, however, that six determinations give practically the same value of the surface gravity (within a factor 2) while the agreement with the trigonometric parallax would require a change of roughly a factor 20 in the surface gravity. It might also be of some interest to note that the only parallax compatible with the spectroscopic gravity is the older McCormick determination (rejected here). To solve this problem, we clearly need a new, accurate, parallax determination. Let us wait for the Hipparcos satellite.

The stellar mass may also, in principle, be estimated by comparing the position of the star in the HR diagram (or a similar one) with theoretical evolutionary tracks. Similarly, the stellar age may be deduced from the comparison of the stellar position in this diagram with representative isochrones. Unfortunately, the uncertainty in the value of the mixing length to use in the stellar evolution calculations makes this procedure somewhat unreliable. In fact, the use of the mixing-length "theory" itself might be questioned (see Sect. 3). We use the evolutionary tracks of Mengel et al. (1979), computed with a mixing length equal to the pressure scale height ($\alpha = l/H_p = 1$), and the isochrones of Ciardullo and Demarque (1977), based on the same stellar evolution calculations. The mass and age estimates are made using the ($T_{\rm eff}$, log$g$) diagram in order to avoid additional uncertainties coming from the trigonometric parallax. The mass fraction of helium is assumed to be $Y = 0.25 \pm 0.05$ and the heavy elements abundance corresponds to $Z = 4\,10^{-4}$ for HD 19445 and $Z = 10^{-4}$ for HD 140283. The results are summarized in Table 6.

It should be pointed out that this value of the mixing length ($\alpha = 1$) is probably too low for Population II as well as Population I stars (see, e.g., Van den Berg, 1983). A value of $\alpha \simeq 1.5$ seems to be more appropriate. While this choice would not change drastically the derived stellar masses, it would result in a significant increase of the stellar ages. In fact, the data do not exclude that

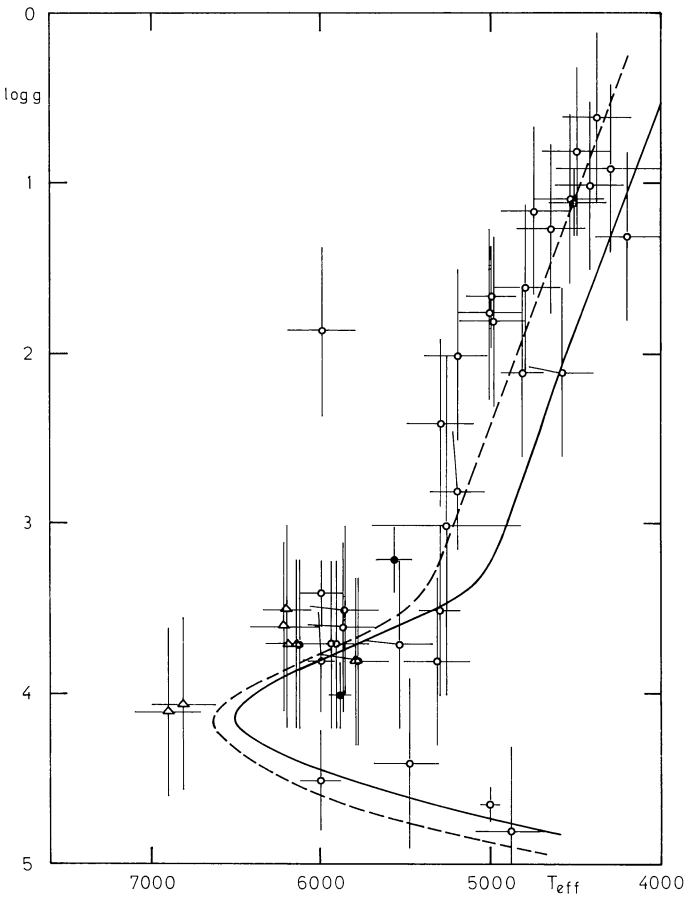

Fig. 7. ($T_{\rm eff}$, log$g$) diagram for stars with [Fe/H] < -1. Full curve: 15 billion years isochrone with $\alpha = 1$. Dashed curve: estimate of the same isochrone with $\alpha = 1.5$. See text for further details

HD 140283 might be at the bottom of the giant branch, in which case its age would be essentially undetermined by the present method. However, it seems impossible to obtain a reasonable age for both stars (say, from 10 to 15 billion years) using the *same* value of the mixing length for both. Part of this problem might be related to the use of the mixing-length "theory": since that "theory" does not provide a satisfactory representation of the atmospheres of those stars, as was shown in Sect. 3, its use in the stellar evolution calculations may introduce non negligible errors. In addition, it should be pointed out that the evolutionary tracks are computed with the assumption that the relative abundances of the heavy elements are solar, which is a rather bad approximation, as will be shown in Sect. 7 below. This might also introduce significant errors in the estimated ages. Note finally that this problem of age determination might be related to the problem reported by Michaud et al. (1984) who show that the evolutionary models are unable to reproduce the Li abundances of the halo stars, as determined by Spite and Spite (1982).

To provide a somewhat better illustration of the position of these stars in the HR diagram, we have plotted in Fig. 7 the representative points of the stars in the Cayrel et al. (1980) catalogue with [Fe/H] < -1, along with the Ciardullo and Demarque (1977) isochrone corresponding to $Y = 0.2$, $Z = 10^{-4}$ and an age of 15 billion years (full curve). The dashed curve corresponds to an estimate of the same isochrone, computed with a mixing length equal to 1.5 (instead of 1) pressure scale height.

The black dots represent the two stars analysed here and the white dots correspond to the stars with $T_{\rm eff}$ and $\log g$ from the Cayrel et al. catalogue. The error bars are estimated in the following way:

– if only one determination of $T_{\rm eff}$ or $\log g$ is available, we adopt $\delta T_{\rm eff}=200$ K and $\delta \log g=0.5$;

– if several determinations are available, the error bars correspond to twice the standard deviation of the mean values.

For some stars, no determination of $\log g$ was reported in the catalogue. In these cases, represented by triangles in Fig. 7, we estimated the surface gravity from the $(b-y, c_1)$ diagram of the Strömgren photometry, using the calibration of Relyea and Kurucz (1978).

The position of the giant branch is very sensitive to the adopted mixing length but completely insensitive to age and only moderately sensitive to Y and Z. It may therefore provide a means of determining the mixing-length parameter α. Note that increasing Z results in a giant branch moving towards lower effective temperatures, thus increasing the discrepancy between the $\alpha=1$ isochrone and the observations. Since the adopted Z value is a lower limit for the sample considered, the position of the giant branch implies that a larger mixing length must be used (at least $\alpha=1.5$, in agreement with the value deduced from the study of globular clusters).

Note, moreover, that the position of HD 140283 at the left of the observed locus is compatible with the fact that this star is one of the most metal-poor ones of the sample considered. The position of HD 19445 seems more peculiar. In Bengt Gustafsson's words, although the location of these two stars in Fig. 7 does not appear improbable, it looks somewhat extreme. Obviously, the complete understanding of the HR diagram of the field metal-poor stars requires further investigations.

7. Relative abundances

This section is devoted to the determination of the abundances of a number of elements in the atmospheres of the two stars considered and to the discussion of some straightforward implications of our results concerning nucleosynthesis and galactic evolution. For the sake of clarity, the elements are grouped according to the process generally considered as mainly responsible for the formation of their dominant isotope in solar system material. Thus, we consider helium burning (producing C, N, and O), carbon burning (Na, Mg, Al), oxygen burning (Si, Ca), silicon burning along with thermonuclear equilibria (responsible for the production of the iron group elements) and the *s* process (Sr, Y, Ba). We are aware that this classification is somewhat arbitrary since a single isotope may sometimes be synthetized by several distinct processes and since the dominant isotope may not be the same in Population I and Population II material.

7.1. The light elements: carbon, nitrogen and oxygen

These are key elements, first because of their high abundances (they are the most abundant after H and He) and, second, as tests of the galactic evolution theories. However, it is relatively difficult to determine their abundances because no line of these atoms is detectable in the visible part of the spectrum. One thus has to go to other spectral regions (e.g., the infrared) or to rely on molecular lines. We determined the carbon abundance from the analysis of the CH band near 4300 Å, while the oxygen abundance was deduced from the O I infrared triplet. On our spectra, the only feature allowing in principle to determine the nitrogen abundance is the CN band near 3880 Å. However, we are not able to derive a reliable abundance from this feature for two reasons:

(1) this band is barely detectable on our spectra, and difficult to measure with sufficient precision;

(2) the dissociation energy of CN is not known with the required accuracy. We consider that the attempts to determine the dissociation energy of CN by fitting synthetic spectra to the observed solar spectrum are subject to the drawbacks of differential analyses discussed in Sect. 4. In particular, it is nearly impossible to locate the continuum in that spectral region. In order to illustrate these problems, we simply mention the fact that Barbuy (1983) finds, for HD 140283, $[N/Fe]\sim+1.0$ from the analysis of the CN band, while Bessel and Norris (1982) obtain $[N/Fe]\sim+0.5$ for the same star by using the NH band near 3360 Å.

No oxygen line is detectable on our spectra, so we use the observations of Sneden et al. (1979) for the O I triplet near 7774 Å, with the oscillator strengths of Wiese et al. (1966) and the solar oxygen abundance recommended by Lambert (1978): $\log A_0=8.92$.

The carbon abundance is derived from the analysis of the (0, 0), (1, 1), and (2, 2) bands of the A – X system of CH near 4300 Å. At a resolution of 0.25 Å, very few lines are isolated, so we have to rely on synthetic spectra. We have selected two spectral regions containing CH lines unperturbed by atomic lines:

(1) $4290\,\text{Å}<\lambda<4300\,\text{Å}$, containing three or four features due to CH alone;

(2) $4322\,\text{Å}<\lambda<4327\,\text{Å}$, containing the head of the $Q(2,2)$ branch, almost unperturbed by other lines.

All significant atomic and molecular lines were taken into account, on the basis of the Moore et al. (1966) catalogue and of the Kurucz and Peytremann (1975) line list. Laboratory oscillator strengths were used as far as possible. When not available, we used the Kurucz and Peytremann values, ajusted if necessary to provide a better match of the solar spectrum. The synthetic spectra were computed by W. Nijs at the Belgium Royal Observatory, with a program written by J. Sauval. The instrumental profile is approximated by a Gaussian, whose width is determined by comparing computed and observed isolated lines. We obtain full widths at half maximum of 0.32 Å for HD 19445 and 0.36 Å for HD 140283, which correspond to a resolution of 0.23 and 0.26 Å, respectively. The oscillator strengths of the different CH bands are taken from Larsson and Siegbahn (1983) and the adopted solar carbon abundance is $\log A_C=8.68$ (Lambert, 1978). Examples of synthetic spectra, computed with three different C abundances, are compared with observations in Fig. 8.

The results are summarized in Table 7, from which two main conclusions may be drawn.

(1) The carbon and iron deficiencies are roughly equal, which confirms the results of previous analyses (Peterson and Sneden, 1978; Barbuy, 1981). This result suggests that C and Fe might be produced during the same event, in contradiction with most existing theories.

(2) Oxygen is strongly overabundant relative to iron and carbon. A similar but less pronounced overabundance has been found by Sneden et al. (1979). These authors, although obtaining [O/H] values practically identical to ours, find $[O/Fe]\sim+0.3$ and $+0.6$ for HD 19445 and HD 140283, respectively. The difference comes from the use of different [Fe/H] values, Sneden et al. adopting the results of Peterson (1978a), which are affected by the systematic errors discussed in Sect. 4. These systematic errors are probably responsible for the peculiar behaviour of [O/Fe] relative

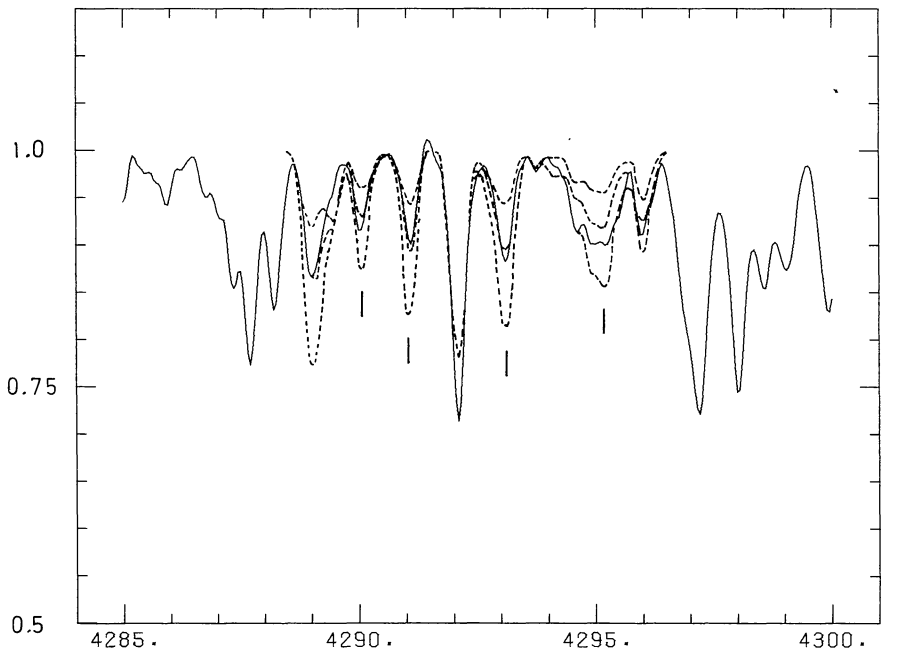

Fig. 8. Comparison of observed (full line) and synthetic (dotted lines) spectra for HD 19445. The features due to CH alone are indicated by the vertical bars. The carbon abundances used in the computations are $\log A_C = 6.1$, 6.4, and 6.7. Same note as for Fig. 5

Table 7. Detailed abundances

Element M	[M/H]		[M/Fe]		σ	
	HD 19445	HD 140283	HD 19445	HD 140283	HD 19445	HD 140283
C	−2.25	−2.76	+0.08	+0.24	–	–
O	−1.56	−1.79	+0.77	+1.21	0.10	0.03
Na	−1.9:	−3.0:	+0.4:	0.0:	0.02	0.19
Mg	−1.84	−2.57	+0.49	+0.43	0.07	0.03
Al	−2.6	−3.7	−0.3	−0.7	–	–
Si	−1.8	−2.5	+0.5	+0.5	–	0.27
Ca	−1.95	−2.62	+0.38	+0.38	0.07	0.04
Ti	−2.07	−2.74	+0.26	+0.26	0.12	0.08
Cr	−2.54	−3.22	−0.21	−0.22	0.04	0.08
Mn	−2.74	−3.44	−0.41	−0.44	0.20	0.05
Fe	−2.33	−3.00	0.00	0.00	0.05	0.04
Co	−2.1:	−2.6:	+0.2:	+0.4:	–	–
Ni	−2.28	−2.92	+0.05	+0.08	0.14	0.13
Sr	−2.0	−3.4	+0.3	−0.4	0.13	0.09
Y	−2.4:	−3.6:	−0.05:	−0.6:	0.16	0.12
Ba	−2.4	−3.9	−0.05	−0.9	–	–

Note: the results marked with a colon should be considered as preliminary

to [Fe/H] noted by Sneden et al. In fact, these authors obtain an oxygen overabundance increasing with the iron deficiency as long as [Fe/H] $\gtrsim -0.5$ and abruptly stabilizing for more metal-poor stars. This sudden change near [Fe/H] $= -0.5$ was difficult to understand. Our results suggest a continuous increase of [O/Fe] as [Fe/H] decreases.

7.2. *Sodium, magnesium and aluminium*

The abundance of Al relative to Mg is a key test of explosive nucleosynthesis theories. It has been discussed in a previous paper (Arpigny and Magain, 1983). The Al abundance was determined from the two violet resonance lines of Al I, while the Mg abundance was deduced from three weak lines of Mg I. The main conclusions were the following.

(1) One of the two lines used for the Al abundance determination (λ3944.0) is perturbed by CH lines. This accounts for the anomalous intensity ratio of these lines in metal-poor stars. The 3944 Å line should not be used to compute the Al abundance.

(2) The overdeficiency of Al relative to Mg is in good agreement with the computations of explosive carbon burning (Arnett, 1971).

(3) The two stars behave in the same way, contrary to what has been stated before (Spite and Spite, 1980; Peterson, 1978b). No special process is thus required to explain a hypothetical difference between hotter and cooler stars.

Note that the small difference between the results of Arpigny and Magain (1983) and those of Table 7 is due to the use of different model atmospheres.

The explosive nucleosynthesis calculations (Arnett, 1971) predict a similar overdeficiency of Na relative to Mg. We have tried to compute the Na abundance from the D lines near 5890 Å. The oscillator strengths are taken from Wiese and Martin (1980), the damping enhancement factor is $f_6 = 1.2$ (Edvardsson, 1983) and the solar Na abundance is $\log A_{NA} = 6.32$ (Lambert and Luck, 1978). In the case of HD 19445, the equivalent widths are measured on the mean of five OHP spectra (emulsion: IIa-D or 098-02, reciprocal dispersion: 20.4 Å mm^{-1}). We obtain 173 and 146 mÅ, respectively. For HD 140283, we use the data of Baschek (1959), who gives 100 mÅ for both lines. We find no significant overdeficiency of Na relative to Mg (Table 7), in contradiction with the behaviour of Al and with the explosive nucleosynthesis calculations. Since the Na equivalent widths are less accurate than the ones we normally use, this result should be considered as preliminary. However, if confirmed, this contradiction would require further investigations. In particular, one should look for possible non-LTE effects in the formation of the Al and Na resonance lines.

7.3. Silicon and calcium

These elements are primarily synthesized during oxygen burning (Cameron, 1973; Trimble, 1975). They belong, with Mg, to the class of "α-elements", which means that their main isotope has the same (even) number of protons and neutrons.

Two Si I lines are measurable on our spectra. The 3905.5 Å line is quite strong: the deduced abundance is thus sensitive to the choice of the damping constant. The 4102.9 Å line is weak but unfortunately situated in the wing of H_δ, which makes the equivalent width measurement rather tricky, especially in the case of HD 140283. We have thus adopted the following procedure for the Si abundance determination. In the case of HD 19445, where the equivalent width of the 4102.9 Å line is reasonably accurate, we derive the Si abundance from this single line. We then determine the damping constant of the 3905.5 Å line by forcing the equality of the abundances deduced from the two lines. We obtain $f_6 = 2.0$. With this value, we may then determine the Si abundance in HD 140283 from this line. The line being slightly weaker in HD 140283, this procedure has the advantage of reducing the uncertainty on the abundance due to the damping constant. The final result for that star is the mean of the abundances deduced from the two lines, with double weight for the weak line. We use the oscillator strengths of Garz (1973) and the solar abundance of Lambert and Luck (1978), namely $\log A_{Si} = 7.63$.

The Ca abundance is determined from 4 weak lines of Ca I, with the oscillator strengths of Smith and O'Neill (1975) and a solar abundance $\log A_{Ca} = 6.36$ (Smith, 1981). The dispersion of the abundances deduced from the 4 lines amounts to some 0.05 dex only, which indicates that both the oscillator strengths and the equivalent widths are of good quality. As expected, the Si abundance is less well determined.

The results are summarized in Table 7, which shows that the "α-elements" are significantly overabundant relative to iron. Note, moreover, the remarkable similarity of the relative abundances in the two stars.

7.4. The iron group elements

The iron group elements (Ti to Ni) are generally considered as being synthesized during explosive silicon burning. The calculations of Arnett (1971) predict an odd-even effect similar to the effect found in the products of explosive carbon burning, although less pronounced. The analysis of this odd-even effect is complicated by the fact that the lines of the elements with an odd number of protons are generally affected by hyperfine structure which, by broadening the lines, may "desaturate" them, in a way similar to microturbulence. The neglect of hyperfine structure may thus cause significant errors.

(1) If the analysis is differential relative to the sun, and if the stellar lines are weak, the solar equivalent widths will be more affected by hyperfine structure. The solar abundance will be overestimated if hyperfine structure is neglected. This will lead to a spurious overdeficiency of the odd elements in the metal-poor stars.

(2) If the analysis is absolute, the result will be an equally spurious underdeficiency of these elements.

For an illustration of these effects, see Beynon (1978b).

The titanium abundance is determined from 4 weak lines of Ti I, with the very accurate oscillator strengths of Blackwell et al. (1982c) and a solar abundance $\log A_{Ti} = 5.10$.

We shall not attempt to derive the vanadium abundance since we lack good oscillator strengths as well as accurately measurable lines.

In the case of chromium, we use 3 Cr I lines (2 for HD 140283). The oscillator strengths are from Blackwell et al. (1984b) and the solar abundance is $\log A_{Cr} = 5.67$ (Biémont et al., 1978).

The manganese abundance is determined from two Mn I resonance lines. The oscillator strengths are from Booth et al. (1984). The hyperfine structure has been accurately determined (Booth et al., 1983) and is taken into account in detail. We use the solar abundance recommended by Grevesse (1984): $\log A_{Mn} = 5.45$.

The iron abundance is computed from a number of Fe I lines with oscillator strengths from the Oxford group (Blackwell et al., 1982a, and references therein). The 2.2 eV lines have been rejected on the basis of their anomalous behaviour (see Paper I and Blackwell et al., 1984a). We adopt the damping constants of Simmons and Blackwell (1982) and a solar abundance $\log A_{Fe} = 7.65$.

The cobalt abundance is determined from the single Co I line at 4121.3 Å, with the oscillator strength of Cardon et al. (1982) and the solar abundance obtained by these authors: $\log A_{Co} = 4.92$. Since we lack accurate hyperfine structure data for that line, we estimate its effect on the Co abundance by adding a fictitious microturbulent velocity. The line being rather weak, the corresponding uncertainty on the Co abundance should not exceed 0.1 dex.

Finally, the nickel abundance is deduced from 8 Ni I lines, with oscillator strengths from the Fuhr et al. (1981) compilation. Since some of these lines are rather strong, we determine the damping constant by forcing the strong lines to give the same abundance as the weaker ones. We obtain $f_6 = 1.75$. In the case of HD 140283, we use the 4 lines measurable on our spectra ($\lambda > 3600$ Å). The solar abundance is taken from Grevesse (1984): $\log A_{Ni} = 6.25$.

The results are summarized in Table 7 which shows that the relative abundances are practically identical in the two stars (within the error bars). Since these results are obtained from lines of neutral elements with similar excitation and ionization potentials, any error on T_{eff} or $\log g$ will leave the relative abundances nearly unchanged. Since, in addition, the dispersion of the results

from different lines of the same element is generally low, the main cause of uncertainty on these relative abundances lies probably in the absolute scale of the oscillator strengths, which is not always accurately known.

The most striking result, apart from the similarity of the relative abundances in the two stars, is the Mn overdeficiency, in agreement with the predictions of explosive nucleosynthesis. This result is also compatible with the conclusions of Beynon (1978a), who proposes the relation $[Mn/Fe] \simeq 0.2\,[Fe/H]$ from the analysis of a sample of Population I stars, with $[Fe/H] > -0.7$. The halo stars thus seem to behave like the disk stars, the Mn abundance varying somewhat more rapidly than the Fe (and other even elements) abundance. The results for Co do not confirm, however, the overdeficiency of the odd elements. Let us recall the similar discrepancy between the Al/Mg and Na/Mg abundance ratios. Nevertheless, it should be pointed out that the Co abundance (as the Na abundance) is less well determined.

Another interesting result is that we find no significant Ni overabundance, in contrast with the results of Luck and Bond (1983) for a sample of metal-deficient giants.

7.5. *The s elements: strontium, yttrium and barium*

It is generally considered that the dominant isotopes of these elements are synthesized by the *s* process, i.e. the slow capture of neutrons by seed nuclei (Burbidge et al., 1957; Trimble, 1975). The rate of formation of these "secondary elements" is predicted to be proportional to the number of seed nuclei, mainly Fe nuclei. The simplest models thus lead to a relation of the type:

$$[s/Fe] \simeq [Fe/H], \qquad (7)$$

where *s* represents any *s* element.

The barium abundance is derived from the only barium line measurable on our spectra, which is the resonance line of Ba II at 4554.0 Å. This line has an equivalent width of 58 mÅ (18 mÅ) in the spectrum of HD 19445 (HD 140283) and is thus well suited for the determination of the Ba abundance. Its oscillator strength is well known from lifetime measurements (Wiese and Martin, 1980). The strontium abundance is deduced from two moderately strong resonance lines of Sr II. The oscillator strengths are from Wiese and Martin (1980) and the damping enhancement factors are assumed to be $f_6 = 1.5$ (as in all cases, unless specified). In the case of yttrium, four weak lines are measurable in the ultraviolet spectrum of HD 19445 but barely detectable in the case of HD 140283. The oscillator strengths are from Hannaford et al. (1982). Since the continuum is relatively poorly defined in that spectral region, the Y abundance should be considered as preliminary. The solar Sr and Ba abundances are taken from Holweger (1979): $\log A_{Sr} = 2.93$ and $\log A_{Ba} = 2.18$, while the Y abundance is from Hannaford et al. (1982): $\log A_Y = 2.24$.

The results may be found in Table 7. The relative abundances $[s/Fe]$ are plotted versus $[Fe/H]$ in Fig. 9. The comparison of the results for the two stars is compatible with Eq. (7), indicating a secondary production of these elements in the halo. However, the comparison with the sun is in complete disagreement with Eq. (7): the straight line of slope unity fitted to the stellar points reaches $[s/Fe] = 0$ at iron deficiencies $[Fe/H] \sim -2$, while the classical models (Tinsley, 1979) predict a curve of slope close to 1 passing through the solar point. This fact has been observed for the first time by Spite and Spite (1978).

According to Twarog (1981), these results indicate an *s* element production some 40 times more efficient in the halo than in the disk. Note that it might equally well indicate an iron production less efficient in the halo than in the disk. If one of these interpretations is correct, the less metal-poor halo stars should show a strong overabundance of *s* elements relative to Fe (for example, $[Sr/Fe] \sim +1.0$ and $[Ba/Fe] \sim +0.6$ at $[Fe/H] \sim -1.5$, these values being obtained by extrapolating our data).

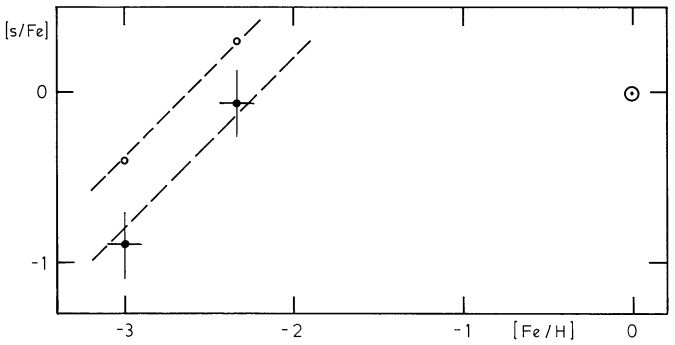

Fig. 9. Plot of [Sr/Fe] (open circles) and [Ba/Fe] (full circles) versus [Fe/H]. The error bars for Sr are similar to those for Ba. The straight lines of slope 1 fitted to the observed points are also represented

Another interpretation has been proposed by Truran (1981), according to whom we are not detecting in the most metal-poor stars the isotopes produced by the *s* process, but the isotopes (less abundant in the solar system) synthesized by the *r* process. This interpretation would allow the most metal-poor stars observed to belong to the second stellar generation, while the observation of secondary elements in their unevolved atmospheres would imply that these stars are members of the third generation. Although this interpretation is very attractive, it does not explain easily the observed variation of $[s/Fe]$ with $[Fe/H]$. Indeed, if the (primary) *r* process isotopes dominate in the metal-poor stars and the (secondary) *s* process isotopes dominate in the Population I stars, one would expect a constant (negative) value of $[s/Fe]$ in the halo stars, followed by a rise towards unit slope in the disk stars. This is just the contrary of the observed behaviour.

Finally, M. Gabriel (private communication) has suggested that this difference of behaviour between the halo and the disk stars might be the consequence of a transition from an *s* elements production limited by the number of seed nuclei (in the halo stars) to a production limited by the number of neutrons available (in the disk stars).

8. Discussion

The relative abundances discussed in the preceding section are summarized in Table 7 and Fig. 10. Also given in Table 7 are the standard deviations of the individual line abundances. These do not correspond, of course, to the total uncertainties on the deduced abundances, but only represent the internal accuracy of our data, mainly equivalent widths and oscillator strengths. As far as the relative abundances are concerned, the total uncertainty should not exceed some 0.1 dex (see Table 11 of Paper I) if there are no significant non-LTE effects or errors on the oscillator strengths. This estimate is valid for the elements with a sufficient number of weak lines (O, Mg, Ca, Ti, Cr, Fe). In particular, the analysis of elements with very accurate relative oscillator strengths, such as Ca and Fe, shows that the uncertainty on the equivalent width of a single weak line is responsible for an uncertainty of roughly 0.05 dex on the abundance.

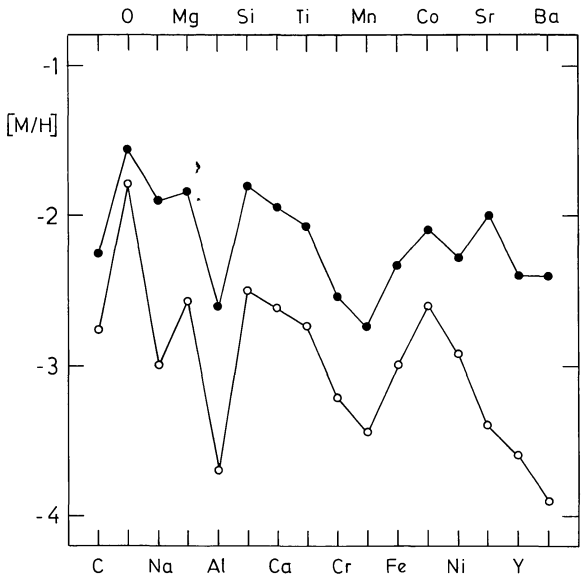

Fig. 10. Abundances of the elements in the atmospheres of HD 19445 (full circles) and HD 140283 (open circles)

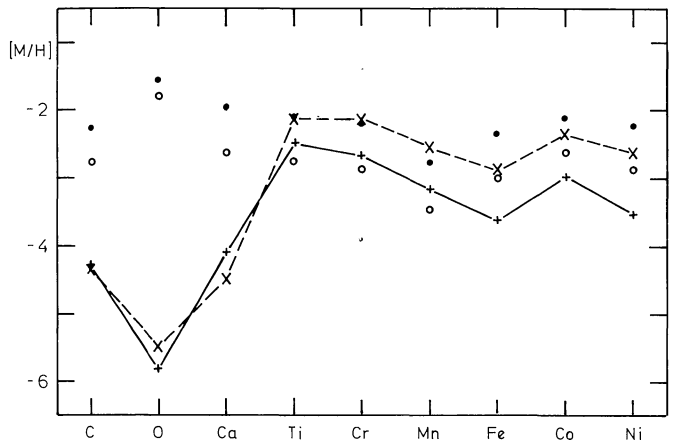

Fig. 11. The abundances of some elements in the atmospheres of HD 19445 (full circles) and HD 140283 (open circles) are compared to the predictions of two SMO models of Wallace and Woosley (1981): × : model *C*, + : model *F*

The first striking result is the similarity of the relative abundances in the two stars analysed. This similarity is even more striking if we consider only the elements with an even number of protons, from Mg to Ni. For these 7 elements, the relative abundances are practically identical: the deficiency of HD 140283 relative to HD 19445 amounts to $-0.68\,(\pm 0.03)$ dex. This 0.03 dex (7%) dispersion is of the same order of magnitude as the error on the mean abundances coming from the equivalent width uncertainties alone. We may thus conclude that, within the accuracy of our analysis, the relative abundances of these elements are identical in the two stars. Comparing now the abundances of these 7 elements in the halo stars with the corresponding values in the sun, Table 7 and Fig. 10 show that the deficiency increases with the atomic number. This trend may be interpreted as indicating a variation of the relative efficiency of the different nucleosynthesis processes when going from the halo to the disk: in the halo, the processes operating at a relatively low temperature (He burning, followed by C and O burnings) would be relatively more efficient than the processes taking place at higher temperatures (Si burning and nuclear equilibria), when compared with the nucleosynthesis processes occurring in the disk.

The Spite[2]-type behaviour of the *s*(?) elements may be considered as another important result of our analysis. In any case, it presents a strong challenge to the galactic evolution theorists. Another important point should nevertheless be mentioned: this is the overabundance of Sr relative to Ba. The *s* process nucleosynthesis calculations (Truran and Iben, 1977) predict that the light *s* elements (e.g. Sr) are formed primarily in rather massive stars ($M > 15\,M_\odot$) while the heavier *s* elements (e.g. Ba) are produced by intermediate mass stars (within 2 and 8 $M_\odot$). The overabundance of Sr relative to Ba would therefore indicate a larger contribution of the massive stars to the nucleosynthesis in the halo than in the disk. This is in agreement with the conclusions drawn from the strong oxygen overabundance. It should be pointed out, however, that these observations do not necessarily imply that the initial mass function has varied through the galactic history, although this interpretation is the most likely. In fact, the shorter lives of the massive stars may quite naturally increase their contribution to the enrichment of the interstellar gas at the very beginning of the galactic evolution.

Apart from the "standard model", according to which most elements are synthesized by the successive stellar generations, other hypotheses have been proposed to account for the distribution of the elements in the halo stars. The most popular of these alternative models suggests that the elements present in the atmospheres of the unevolved halo stars have been synthesized by pregalactic "super massive objects" (SMO). Such objects, with masses $M \gtrsim 10^3\,M_\odot$, would be able to produce most elements in quantities roughly comparable to the abundances observed in the most metal-deficient stars. However, the computations do not fit at all the observed relative abundances, as is shown in Fig. 11 where the abundances of a number of elements in the stars considered are compared to the predictions of two typical SMO models (Wallace and Woosley, 1981). The disagreement between the models and the observations is especially strong for the lighter elements, such as C, O, and Ca.

Our results thus suggest that the standard model provides the best fit to the observations, which confirms the conclusions of most (if not all) recent analyses. It should be pointed out, however, that the strength of that model lies primarily in the weakness of its predictions. By this we mean that this model involves such a large number of different processes occuring in different objects or in different circumstances that it does not lend itself to really decisive tests: it is really hard to find any result which might be in clear contradiction with some definite prediction of that model. If confirmed, however, some results of our analysis might constitute a severe challenge for that model. Let us simply recall the probable contradiction between the Al/Mg and Na/Mg abundance ratios, as well as between the Mn/Fe and Co/Fe ratios, or the Spite[2]-type behaviour of the *s* elements.

At the present stage, it seems to us that any significant progress in the understanding of the early chemical evolution of the Galaxy will come from the accurate analysis of a sufficient number of representative stars. It is clear to us that the stellar spectroscopists interested in the halo stars should put the emphasis on the quality of the observational data, and not on the quantity, as was often the case in the past. The best way to slow down our progress in the understanding of the early stages of the galactic evolution is to swamp the theorists with unreliable data. As is illustrated in Table 8 and in Fig. 2 of Arpigny and Magain (1983), many analyses (including recent ones) do not give sufficiently reliable

Table 8. Comparison of the relative abundances [M/Fe] obtained by different authors

Element	AG	CS	S^2	P	M
a) HD 19445					
C	−0.50:			−0.15	+0.08
Mg	+1.17	+0.74	+1.0?	+0.11	+0.49
Al	+0.21:	−0.02	+0.4	−1.01	−0.3
Si	+0.55:	+0.58			+0.5
Ca	+0.38	+0.24		+0.43	+0.38
Ti	+0.39	+0.24		+0.19	+0.26
Cr	+0.07	−0.06			−0.21
Mn	+0.21	+0.34			−0.41
Co	+1.2:	+0.81			+0.2:
Ni	+0.22	−0.45			+0.05
Sr	−0.17				+0.3
Ba	−0.40	−0.20	−0.3		−0.05
b) HD 140283					
C	−1.42:	+0.65		+0.10	+0.24
Mg	+0.12	+0.52	−0.3	−0.12	+0.43
Al	−0.75:	−0.77	−0.6	−0.20	−0.7
Si	−0.25	+0.20			+0.5
Ca	−0.04	+0.54			+0.38
Ti	+0.20	+0.33			+0.26
Cr	+0.39	+0.28			−0.22
Mn	−0.01	−0.10			−0.44
Co	+0.54	+0.02			+0.4:
Ni	+0.57	+0.47			+0.08
Sr	−0.05				−0.4
Y	−0.61:	−0.22	−0.4		−0.6:
Ba	−0.61	−0.86	−0.8		−0.9

Notes to Table 8
(1) AG = Aller and Greenstein (1960); CS = Cohen and Strom (1968); S^2 = Spite and Spite (1978); P = Peterson (1981) or Peterson and Sneden (1978); M = this paper
(2) If the abundance is determined from the two ionization stages, we adopt the mean of the two values
(3) In the case of CS, we adopt the mean of the results obtained with the two selected models

results. Even for such unpeculiar elements as Mg, Fe, and Ni, the results of different authors may disagree by as much as an order of magnitude.

As already indicated in the Introduction, our aim was not only (1) to realise a detailed and accurate analysis of representative halo dwarfs in view of providing the theorists with reliable observational data, but also (2) to shed some light on the possible uncertainties or drawbacks of past analyses. As far as point (1) is concerned, we hope that our work has allowed to improve the general knowledge of the halo dwarfs. However, some points clearly need further investigations. First, as Sect. 6 has shown, our understanding of the evolution of these stars may be far from satisfactory. Second, it would be very interesting to obtain the abundances of the *s* elements in a sample of halo dwarfs with different iron abundances, and especially in the less metal-poor halo stars. Third, the Al/Mg, Na/Mg, Mn/Fe, and Co/Fe abundance ratios need further investigations, using non-resonance weak lines if possible. It would also be very interesting to obtain reliable nitrogen abundances in the extreme halo dwarfs. And, finally, the effects of convection on the atmospheric structure of these stars should be investigated with the help of high resolution observations of line profiles and of sophisticated models such as Nordlund (1982) numerical simulations.

Acknowledgements. Our thanks are due to C. Arpigny, M. Gabriel, N. Grevesse, B. Gustafsson and M. Spite for stimulating discussions. We also wish to thank B. Gustafsson for allowing us to use a copy of his model atmosphere program, L. Delbouille for help with the HP 2100 computer and J. Bosseloirs who kindly made the drawings.

Appendix. Equivalent widths

The line equivalent widths measured on our spectra are given in Table A1. The wavelengths λ are in Å, the excitation potentials χ in eV and the equivalent widths W_λ in mÅ. In the case of HD 140283, the equivalent widths of the lines with $\lambda < 3900$ Å are the mean of the values measured on the OHP and ESO spectra, the latter being corrected according to Eq. (1). All other equivalent widths are measured on the OHP spectra. The values marked with a colon are less accurate.

Table A1. Equivalent widths

λ	Element	χ	$\log(gf)$	Source	W_λ(19445)	W_λ(140283)
3515.1	Ni I	0.11	−0.24	(4)	146	
3549.0	Y II	0.13	−0.28	(10)	12	
3551.5	Ni I	0.17	−2.56	(4)	22	
3566.4	Ni I	0.42	−0.27	(4)	131	
3597.7	Ni I	0.21	−1.08	(4)	84	
3611.0	Y II	0.13	+0.01	(10)	28	
3619.4	Ni I	0.42	0.00	(4)	134	116
3710.3	Y II	0.18	+0.46	(10)	29	10:
3774.3	Y II	0.13	+0.22	(10)	27	10:
3775.6	Ni I	0.42	−1.35	(4)	65	58
3783.5	Ni I	0.42	−1.31	(4)	84	72
3820.4	Fe I	0.86	+0.119	(1)	260	183
3825.9	Fe I	0.91	−0.037	(1)	209	160
3858.3	Ni I	0.42	−0.97	(4)	85	76
3859.9	Fe I	0.00	−0.710	(1)	250	179

Table A1 (continued)

λ	Element	χ	$\log(gf)$	Source	W_λ(19445)	W_λ(140283)
3905.5	Si I	1.91	−1.09	(2)	224	179
3906.5	Fe I	0.11	−2.243	(1)	110	83
3920.3	Fe I	0.12	−1.746	(1)	117	114
3922.9	Fe I	0.05	−1.651	(1)	135	129
3944.0	Al I	0.00	−0.64	(3)	140	95
3950.0	Fe I	2.18	−1.154	(1)	35	28
3958.2	Ti I	0.05	−0.157	(1)	43	21
3961.5	Al I	0.01	−0.34	(3)	123	80
3989.8	Ti I	0.02	−0.188	(1)	39:	25:
3998.6	Ti I	0.05	−0.046	(1)	43	22
4005.2	Fe I	1.56	−0.610	(1)	119	86
4021.9	Fe I	2.76			42	29
4028.4	Ti II	1.89	−0.87	(5)	26	19:
4033.1	Mn I	0.00	−0.618	(1)	76	72
4034.5	Mn I	0.00	−0.811	(1)	74	52
4044.6	Fe I	2.83			22	16
4045.8	Fe I	1.48	+0.280	(1)	263	167
4057.5	Mg I	4.34	−0.89	(7)	48	18
4062.5	Fe I	2.84			31	21
4063.6	Fe I	1.56			178	114
4068.0	Fe I	3.21			32	24
4071.8	Fe I	1.61	−0.022	(1)	155	117
4073.8	Fe I	3.26			18	15
4074.8	Fe I	3.05			20	19
4077.7	Sr II	0.00	+0.15	(6)	117	79
4078.4	Fe I	2.61			17	16
4102.9	Si I	1.91	−3.14	(2)	37:	19:
4121.3	Co I	0.92	−0.32	(8)	37	34
4126.2	Fe I	3.33			16	7:
4132.1	Fe I	1.61			109	83
4132.9	Fe I	2.84			28:	10
4137.0	Fe I	3.41			18	16
4143.4	Fe I	3.05			51	32
4143.9	Fe I	1.56			113	98
4147.7	Fe I	1.48	−2.104	(1)	39	26
4153.9	Fe I	3.40			32	17
4154.5	Fe I	2.83			41	25
4154.8	Fe I	3.37			23:	23
4157.8	Fe I	3.42			22	14
4167.3	Mg I	4.34	−0.71	(7)	56	23
4174.9	Fe I	0.91	−2.969	(1)	17	20
4175.6	Fe I	2.84			30	18
4176.6	Fe I	3.37			20	13
4178.9	Fe II	2.58	−2.60	(9)	25	16
4181.8	Fe I	2.83			53	33
4187.1	Fe I	2.45	−0.548	(1)	71	49
4187.8	Fe I	2.42	−0.554	(1)	71	51
4191.4	Fe I	2.42			56	47
4195.3	Fe I	3.33			26	15
4199.1	Fe I	3.05			61	54
4202.0	Fe I	1.48	−0.708	(1)	110	98
4213.7	Fe I	2.84			19	13
4215.5	Sr II	0.00	−0.17	(6)	109	64
4216.2	Fe I	0.00	−3.356	(1)	42	38
4217.6	Fe I	3.43			26	11
4222.2	Fe I	2.45	−0.967	(1)	46	29
4224.2	Fe I	3.37			28	18
4226.7	Ca I	0.00	+0.24	(6)	313	166

Table A1 (continued)

λ	Element	χ	$\log(gf)$	Source	W_λ(19445)	W_λ(140283)
4227.4	Fe I	3.33			72:	53
4231.0	Ni I	3.54			22	20
4233.2	Fe II	2.58	−1.84	(9)	49	44
4233.6	Fe I	2.48	−0.604	(1)	62	47
4235.9	Fe I	2.42	−0.341	(1)	96	77:
4238.8	Fe I	3.40			37	26
4246.8	Sc II	0.31			76	66
4250.1	Fe I	2.47	−0.405	(1)	66	56
4254.4	Cr I	0.00	−0.108	(1)	82	73
4260.5	Fe I	2.40			118	81
4271.2	Fe I	2.45	−0.349	(1)		62:
4271.8	Fe I	1.49	−0.164	(1)	150:	105
4282.4	Fe I	2.18			58	54
4283.0	Ca I	1.89			50	42
4289.4	Ca I	1.88			46	30:
4289.7	Cr I	0.00	−0.388	(1)	73	57
4290.2	Ti II	1.16	−0.95	(5)	55:	46:
4320.7	Sc II	0.61			26	29
4321.0	Ti II	1.16	−1.89	(5)	23:	13:
4325.8	Fe I	1.61			153	125:
4369.8	Fe I	3.05			30	19
4371.3	Cr I	1.00				15
4375.9	Fe I	0.00	−3.031	(1)	61	52
4383.6	Fe I	1.48	+0.200	(1)	222	133
4394.1	Ti II	1.22	−1.67	(5)	19:	11:
4395.0	Ti II	1.08			72	60
4399.8	Ti II	1.24	−1.29	(5)	42	29
4400.4	Sc II	0.61			23	14:
4404.8	Fe I	1.56	−0.142	(1)	171	115
4415.1	Fe I	1.61	−0.615	(1)	103	88
4416.8	Fe II	2.78	−2.54	(9)	24	13
4417.7	Ti II	1.16	−1.16	(5)	44	32
4418.3	Ti II	1.24	−2.25	(5)	17:	10:
4425.4	Ca I	1.88	−0.358	(1)	40	20
4427.3	Fe I	0.05	−3.044	(1)	62	51
4430.6	Fe I	2.22	−1.659	(1)	20	13
4435.0	Ca I	1.89	−0.007	(1)	65	38
4435.7	Ca I	1.89	−0.517	(1)	30	17
4442.4	Fe I	2.20	−1.255	(1)	41	23
4443.8	Ti II	1.08	−0.69	(5)	71	64
4444.6	Ti II	1.12	−2.22	(5)	12:	9:
4447.7	Fe I	2.22	−1.342	(1)	39	24
4453.3	Ti I	1.43			10:	
4454.8	Ca I	1.90	+0.258	(1)	85	51
4461.7	Fe I	0.09	−3.210	(1)	53	45
4466.6	Fe I	2.83			37	31
4468.5	Ti II	1.13	−0.61	(5)	74	63
4469.4	Fe I	3.65			13:	10
4484.2	Fe I	3.60			16	14
4489.8	Fe I	0.12	−3.966	(1)	18	12
4491.4	Fe II	2.85			9	
4494.6	Fe I	2.20	−1.136	(1)	44	27
4501.3	Ti II	1.12	−0.74	(5)	69	58
4508.3	Fe II	2.85	−2.33	(9)	17	14
4515.3	Fe II	2.84	−2.49	(9)	22	8:
4518.0	Ti I	0.83	−0.325	(1)	12	
4520.2	Fe II	2.81	−2.55	(9)	16	12
4522.6	Fe II	2.84				26

Table A1 (continued)

λ	Element	χ	$\log(gf)$	Source	W_λ(19445)	W_λ(140283)
4528.6	Fe I	2.18	−0.822	(1)	65	46
4531.2	Fe I	1.48	−2.155	(1)	26	22
4533.3	Ti I	0.85	+0.476	(1)	26	18
4534.0	Ti II	1.24	−0.64	(5)	72	59
4534.8	Ti I	0.84	+0.280	(1)	15	12:
4554.0	Ba II	0.00	+0.163	(6)	58	18
4555.9	Fe II	2.83	−2.39	(9)	14	10
4563.8	Ti II	1.22	−0.82	(5)	61	42
4572.0	Ti II	1.57	−0.34	(5)	72	52
4583.8	Fe II	2.81				36
4603.0	Fe I	1.48	−2.220	(1)	31	19
4646.2	Cr I	1.03	−0.727	(1)	12	
4703.0	Mg I	4.34	−0.38	(7)	91	42

Note to Table A1. The sources of oscillator strengths are the following: (1) Oxford group (Blackwell and collaborators); (2) Garz (1973); (3) Wiese et al. (1969); (4) Fuhr et al. (1981); (5) gf values selected for Ti II (see Sect. 5); (6) Wiese and Martin (1980); (7) Froese-Fisher (1975); (8) Cardon et al. (1982); (9) Moity (1983) corrected (see Sect. 5); (10) Hannaford et al. (1982)

References

Aller, L.H., Greenstein, J.L.: 1960, *Astrophys. J. Suppl.* **5**, 139
Arnett, W.D.: 1971, *Astrophys. J.* **166**, 153
Arpigny, C., Magain, P.: 1983, *Astron. Astrophys.* **127**, L7
Barbuy, B.: 1981, *Astron. Astrophys.* **101**, 365
Barbuy, B.: 1983, *Astron. Astrophys.* **123**, 1
Baschek, B.: 1959, *Z. Astrophys.* **48**, 95
Beckers, J.M., Bridges, C.A., Gilliam, L.B.: 1976, *Air Force Geophys. Lab.* Tech. Rept., No. 76-0126
Bessel, M.S., Norris, J.: 1982, *Astrophys. J. Letters* **263**, L29
Beynon, T.G.R.: 1978a, *Astron. Astrophys.* **64**, 145
Beynon, T.G.R.: 1978b, *Astron. Astrophys.* **64**, 299
Biémont, E., Grevesse, N., Huber, M.C.E.: 1978, *Astron. Astrophys.* **67**, 87
Blackwell, D.E., Shallis, M.J.: 1977, *Monthly Notices Roy. Astron. Soc.* **180**, 177
Blackwell, D.E., Petford, A.D., Shallis, M.J., Simmons, G.J.: 1982a, *Monthly Notices Roy. Astron. Soc.* **199**, 43
Blackwell, D.E., Menon, S.L.R., Petford, A.D.: 1982b, *Monthly Notices Roy. Astron. Soc.* **201**, 603
Blackwell, D.E., Menon, S.L.R., Petford, A.D., Shallis, M.J.: 1982c, *Monthly Notices Roy. Astron. Soc.* **201**, 611
Blackwell, D.E., Booth, A.J., Petford, A.D.: 1984a, *Astron. Astrophys.* **132**, 236
Blackwell, D.E., Menon, S.L.R., Petford, A.D.: 1984b, *Monthly Notices Roy. Astron. Soc.* **207**, 533
Booth, A.J., Shallis, M.J., Wells, M.: 1983, *Monthly Notices Roy. Astron. Soc.* **205**, 191
Booth, A.J., Blackwell, D.E., Petford, A.D., Shallis, M.J.: 1984, *Monthly Notices Roy. Astron. Soc.* **209**, 77
Burbidge, E.M., Burbidge, G.R., Fowler, W.A., Hoyle, F.: 1957, *Rev. Mod. Phys.* **29**, 547
Cameron, A.G.W.: 1973, *Space Sci. Rev.* **15**, 121
Cardon, B.L., Smith, P.L., Scalo, J.M., Testerman, L., Whaling, W.: 1982, *Astrophys. J.* **260**, 395
Carney, B.W.: 1983, *Astron. J.* **88**, 623
Cayrel de Strobel, G., Bentolila, C., Hauck, B., Curchod, A.: 1980, *Astron. Astrophys. Suppl.* **41**, 405
Ciardullo, R.B., Demarque, P.: 1977, *Trans. Yale Univ. Obs.*, Vol. 33
Cohen, J.G., Strom, S.E.: 1968, *Astrophys. J.* **151**, 623
Danzmann, K., Kock, M.: 1980, *J. Phys.* B **13**, 2051
Delbouille, L., Neven, L., Roland, G.: 1973, Photometric Atlas of the Solar Spectrum from 3000 Å to 10,000 Å, Institut d'Astrophysique de l'Université de Liège, Belgium
Edvardsson, B.: 1983, *Uppsala Astron. Obs. Rep.* No. 27
Froese-Fisher, C.: 1975, *Canadian J. Phys.* **53**, 184
Fuhr, J.R., Martin, G.A., Wiese, W.L., Younger, S.M.: 1981, *J. Phys. Chem. Ref. Data* **10**, 305
Garz, T.: 1973, *Astron. Astrophys.* **26**, 471
Gray, D.F.: 1976, The Observation and Analysis of Stellar Photospheres, Wiley, New York
Grevesse, N.: 1984, *Physica Scripta* T **8**, 49
Gustafsson, B.: 1980, ESO Workshop on Methods of Abundance Determination for Stars, Geneva, p. 31
Gustafsson, B., Bell, R.A., Eriksson, K., Nordlund, Å.: 1975, *Astron. Astrophys.* **42**, 407
Hannaford, P., Lowe, R.M.: 1982, *J. Phys.* B **16**, L43
Hannaford, P., Lowe, R.M., Grevesse, N., Biémont, E., Whaling, W.: 1982, *Astrophys. J.* **261**, 736
Holweger, H.: 1979, Les Elements et leurs Isotopes dans l'Univers, eds. A. Boury, N. Grevesse, L. Remy-Battiau, Institut d'Astrophysique de l'Université de Liège, p. 117
Holweger, H., Müller, E.A.: 1974, *Solar Phys.* **39**, 19
Ianna, P.A., McAlister, H.A.: 1974, *Astron. J.* **79**, 1314
Jenkins, L.F.: 1952, General Catalogue of Trigonometric Parallaxes, Yale Univ. Obs. Edition
Kurucz, R.L.: 1979, *Astrophys. J. Suppl.* **40**, 1
Kurucz, R.L., Peytremann, E.: 1975, SAO Spec. Rept. 362
Lambert, D.L.: 1978, *Monthly Notices Roy. Astron. Soc.* **182**, 249
Lambert, D.L., Luck, R.E.: 1978, *Monthly Notices Roy. Astron. Soc.* **183**, 79
Larsson, M., Siegbahn, P.E.M.: 1983, *J. Chem. Phys.* **79**, 2270
Luck, R.E., Bond, H.E.: 1983, *Astrophys. J.* **271**, L75
Magain, P.: 1983, *Astron. Astrophys.* **122**, 225
Magain, P.: 1984a, Thesis
Magain, P.: 1984b, *Astron. Astrophys.* **132**, 208 (Paper I)

Magain, P.: 1984c, *Astron. Astrophys.* **134**, 189
Mengel, J.G., Sweigart, A.V., Demarque, P., Gross, P.G.: 1979, *Astrophys. J. Suppl.* **40**, 733
Michaud, G., Fontaine, G., Beaudet, G.: 1984, *Astrophys. J.* **282**, 206
Moity, J.: 1983, *Astron. Astrophys. Suppl.* **52**, 37
Moore, C.E., Minnaert, M.G.J., Houtgast, J.: 1966, NBS Monogr. No. 61
Nordlund, Å.: 1982, *Astron. Astrophys.* **107**, 1
Oke, J.B., Gunn, J.E.: 1983, *Astrophys. J.* **266**, 713
Peterson, R.C.: 1978a, *Astrophys. J.* **222**, 181
Peterson, R.C.: 1978b, *Astrophys. J.* **222**, 595
Peterson, R.C.: 1981, *Astrophys. J.* **244**, 989
Peterson, R.C., Carney, B.W.: 1979, *Astrophys. J.* **231**, 762
Peterson, R.C., Sneden, C.: 1978, *Astrophys. J.* **225**, 913
Relyea, L.J., Kurucz, R.L.: 1978, *Astrophys. J. Suppl.* **37**, 45
Sauval, A.J., Grevesse, N., Brault, J.W., Stokes, G.M., Zander, R.: 1984, *Astrophys. J.* **282**, 330
Simmons, G.J., Blackwell, D.E.: 1982, *Astron. Astrophys.* **112**, 209
Smith, G.: 1981, *Astron. Astrophys.* **103**, 351
Smith, G., O'Neill, J.A.: 1975, *Astron. Astrophys.* **38**, 1
Sneden, C., Lambert, B.L., Whitaker, R.W.: 1979, *Astrophys. J.* **234**, 964
Spite, M., Spite, F.: 1978, *Astron. Astrophys.* **67**, 23
Spite, M., Spite, F.: 1980, *Astron. Astrophys.* **89**, 118
Spite, F., Spite, M.: 1982, *Astron. Astrophys.* **115**, 357
Tinsley, B.M.: 1979, *Astrophys. J.* **229**, 1046
Trimble, V.: 1975, *Rev. Mod. Phys.* **47**, 877
Truran, J.W.: 1981, *Astron. Astrophys.* **97**, 391
Truran, J.W., Iben, I.: 1977, *Astrophys. J.* **216**, 797
Twarog, B.A.: 1981, *Astrophys. J.* **250**, 753
Van den Berg, D.A.: 1983, *Astrophys. J. Suppl.* **51**, 29
Wallace, R.K., Woosley, S.E.: 1981, *Astrophys. J. Suppl.* **45**, 389
Wiese, W.L., Glennon, B.M., Smith, M.W.: 1966, Atomic Transition Probabilities, NSRDS-NBS-4
Wiese, W.L., Fuhr, J.R.: 1975, *J. Phys. Chem. Ref. Data* **4**, 263
Wiese, W.L., Martin, G.A.: 1980, NSRDS-NBS-68
Wolnik, S.J., Berthel, R.O.: 1973, *Astrophys. J.* **179**, 665